RSC Advances

ROYAL SOCIETY OF CHEMISTRY

www.rsc.org/advances

Journal Name

RSCPublishing

ARTICLE

In situ Nano-Fibrillation of Microinjection Molded Poly(lactic acid)/Poly(ε-caprolactone) Blends and Comparison with Conventional Injection Molding

Cite this: DOI: 10.1039/x0xx00000x

Received 00th July 2015,
Accepted 00th July 2015

DOI: 10.1039/x0xx00000x

www.rsc.org/

Weiwei Ding[a], Yinghong Chen[a]*, Zhuo Liu[a], Sen Yang[a]

In this paper, the microinjection molding (μIM) of poly(lactic acid) (PLA)/poly(ε-caprolactone) (PCL) blend as well as a full comparison with the conventional injection molding (CIM) was carried out. The prepared PLA/PCL blend micropart and macropart were characterized by using various measurements. The results showed that μIM and CIM have the significantly different influence on the structure and performance of PLA/PCL blend. μIM leads to the remarkable reduction in the domain size of PCL dispersed phase to nanometer range, improvement in interfacial compatibility and narrower domain size distribution. Very interestingly, there are PCL nano fibrils *in situ* formed and oriented along melt flow direction in μIM micropart, i.e. occurrence of *in situ* PCL nano-fibrillation phenomenon. Comparatively, only PCL micro fibrils are formed in CIM macropart, i.e. occurrence of PCL micro-fibrillation. For both micropart and macropart, the shear layer shows the much higher degrees of PCL nano/micro-fibrillation and orientation than the core layer. Compared with macropart, micropart exhibits the increased PCL crystallinity and the remarkably enhanced PLA crystallization capability. μIM also leads to higher PLA degradation degree than CIM. In addition, PLA/PCL blend micropart shows much higher mechanical performance and much more obvious double yielding phenomenon than macropart.

1. Introduction

With the rapid development of modern science and technology, there are the increasing requirements for the miniaturized and functionalized products in various high technology fields. The micro device products with the advantages of versatility and easy mass-production have been growing rapidly in the past few decades.[1] Among the microprocessing technologies, microinjection molding (μIM) has become the most commonly used micro molding methods (especially for polymer materials) because of its relatively low cost and accurate replication in preparation of some products with micro-structured features.[2-4] Currently, polymer micro components are being more and more widely applied in many important areas such as automobile manufacturing, electronic communication, precision machinery, biomedical engineering, etc.,[5-6] because polymer materials possess excellent processability, good comprehensive mechanical performance and good replication performance.

The current study on microinjection molding technology in literatures was mainly focused on mold structure optimization,[7-9] melt flowing and filling behavior in the micro-flow channel,[10-13] process parameters,[14] apparent quality and microstructure of micropart,[15-19] etc.. However, the investigations of the properties (especially mechanical performance) of microinjection molding products are relatively less involved, which is possibly related to the too small dimension of the microparts. Below are several examples.[20-22] Huang et al[20] prepared polypropylene (PP) products with thickness of 0.7 mm (μ-PP) and 3.5 mm (m-PP) through microinjection molding and conventional injection molding, respectively. The results showed that compared with m-PP products, tensile strength and storage modulus (40 °C) of μ-PP increases by 67% and 48% respectively. Pan et al[21] compared the structure distribution and tensile property of microinjection molded and conventional injection molded isotactic polypropylene. The results showed that microparts have higher orientation degree and crystallinity as compared to macroparts, resulting in the remarkably enhanced tensile strength and modulus (e.g. increasing from

[a] State Key Laboratory of Polymer Materials Engineering, Polymer Research Institute, Sichuan University, Chengdu 610065, China. E-mail: johnchen@scu.edu.cn; Tel: +86 28 85405136; Fax: +86 28 85402465

35.8 and 240 MPa for macroparts to 46.5 and 1540 MPa for microparts, respectively). Lin et al[22] analyzed the yield strength and elongation at break of the microinjection molded HDPE samples and found that increasing the injection rate, elevating mold temperature and prolonging cooling time can increase the yield strength of HDPE.

Relative to conventional injection molding (CIM), the melt in microinjection molding (μIM) shows larger shear rate, temperature gradient and quicker cooling rate, which could make the μIM products exhibit unique morphology different from the CIM products. This would necessarily affect the mechanical properties of the microparts.[17, 23, 24] This paper will deal with the microinjection molding problem of PLA/PCL blend system and make a comparison with conventional injection molding. As is well known, poly(lactic acid) (PLA) is a biodegradable aliphatic polyester and is derived from the natural material such as potato, corn, etc. As one of the environmental friendly biodegradable polymers, PLA exhibits excellent mechanical properties (can be comparable to PS, PC, etc.), good formability, fast degradation rates and good biocompatibility,[25] which promote its applications in drug delivery system, absorbable surgical suture, tissue engineering scaffold and biomedical microdevice.[26-28] However, the characteristics of low crystallinity and rigid structural skeleton[29] and the existence of tertiary carbon atoms would result in brittleness, poor heat resistance and easy decomposition of PLA during processing,[30-31] which greatly limits its more broad application. As a result, copolymerization or blend of PLA with a tough polymer is an effective approach to improve its toughness.[32] As we know, poly(ε-caprolactone) (PCL) is also a biodegradable and biocompatible polyester with excellent flexibility and formability, but its insufficient strength and high cost are still the factors hindering its wider applications.[33] So, melt blending of PLA with flexible PCL to achieve the performance complementarity is one of the most cost-effective approaches to expand their application fields. Because of this, in recent years, there is much work on PLA/PCL blend carried out.[34-39] For example, Jen-Taut Yeh et al[35] found that PCL promoted the crystallization of PLA as a nucleating agent and also played a toughening role for PLA. Semba et al[36] conducted cross-linking of PLA/PCL blends and found strong interfacial interactions formed between the PLA and PCL phase, resulting in the increase of elongation at break. Bai et al[38] utilized a nucleating agent to tailor the crystallization of PLLA in the blend of PLLA/PCL (80/20) and got a wide range of matrix crystallinity (10−50%) by altering the nucleating agent concentrations and mold temperatures. However, in the publications related to PLA/PCL blend, there is no research conducted on microinjection molding of PLA/PCL blend. So, it would be of great interest to investigate the microinjection molded PLA/PCL blend system.

In this paper, PLA/PCL blends were accordingly prepared and are used for the microinjection molding processing. In general, the morphology and thermal behavior of semicrystalline materials strongly affect their mechanical properties. As a result, the variations in phase morphology, crystallization and tensile property of PLA/PCL blends under microinjection molding conditions were investigated. In addition, the comparisons of the morphology and structure evolution between μIM micropart and CIM macropart were also carried out by means of SEM, DSC and WAXD characterizations. Very interestingly, there are nano PCL fibrils *in situ* formed during microinjection molding process, which is for the first time reported by us. The formation of PCL nanofibrils is beneficial to the high performance of PLA/PCL blend.

2. Experimental

2.1 Materials and sample preparation

The commercially available poly(lactic acid) (trade name 4032D and $M_w \approx 10^6$) was purchased from UNIC Technology Co., Ltd. (Suzhou, China). The used PLA has the glass transition temperature of 50-55°C, melting temperature of 165-170°C and melting flow index of 3.87 g/min (190°C, 2.16Kg load). Poly(ε-caprolactone) (trade name 600c and M_w=60000) with the melting temperature of about 60°C and glass transition temperature of about -60°C was supplied by Shenzhen Brightchina Industrial Co. (China). The used 1 wt% sodium hydroxide (NaOH) solution was self-formulated.

In order to avoid the hydrolysis of raw material induced by water absorption during processing, the PLA and PCL pellets were dried under vacuum at 40 °C for 24 hours. The dried PLA and PCL pellets with a weight ratio of 80/20 were first mixed in a high-speed mixer and then extruded in a TSSJ-25/33 twin-screw extruder (ϕ=25 mm, L/D=33, Chenguang Research Institute of Chemical Industry, China) with a screw rotation speed of 80 rpm at 175 °C. The cooled extrudates were cut into pellets and then dried under vacuum at 40 °C for 24 hours. Finally, the dried PLA/PCL blend pellets were injection-molded into microparts and macroparts at melt temperature of 180 °C and mold temperature of 40 °C by using a MicroPower5 microinjection molding machine (Wittmann Battenfeld GmbH, Austria)[15] and K-TEC 40 conventional injection molding machine (Terromatik Milacron Corporation, USA), respectively. Fig. 1 (a-b) and (c) show the dimension and geometry of the micropart and macropart, respectively. To evaluate the tensile property of PLA/PCL microparts, the dumbbell-shaped microparts were used and the corresponding dimension and geometry are shown in Fig. 1 (d).

2.2 SEM measurements

Scanning electronic microscopy (SEM) analysis was conducted on both PLA/PCL blend microparts and macroparts. First, in order to let the PLA/PCL blend microparts and macroparts fully frozen, they were immerged in liquid nitrogen for about 30 min and then fractured along both the cross-section and melt flow direction. The fractured surface of the samples along the melt flow direction was etched using a 1 wt% sodium hydroxide solution for 8 hours so as to remove parts of PLA phase. The quench-fractured surfaces of all samples were

coated with a thin layer of gold by vacuum spraying, and observed using an INSPECT F (FEI Company, Japan) scanning electron microscope with an accelerating voltage of 5 kV.

2.3 DSC characterization

A TA Q20 differential scanning calorimeter (DSC) (TA Company, USA) was used to analyze the melting and crystallization behavior of PLA/PCL microparts and macroparts. About 6~8 mg samples were first cooled from 40 °C to 0 °C at a cooling rate of 10 °C/min and then heated to 200℃ at a heating rate of 10 °C/min with a dynamic nitrogen gas flow rate of 50ml/min. The corresponding melting and crystallization curves were accordingly recorded. The relative crystallinity degree of PLA and PCL in the blend could be obtained using the following formula, respectively:

$$X_{c,\,PLA}=\frac{\Delta H_{m,\,PLA}-\Delta H_{c,\,PLA}}{\Delta H_{0,\,PLA}\cdot\omega_{PLA}}\times 100\% \quad (1)$$

$$X_{c,\,PCL}=\frac{\Delta H_{m,\,PCL}}{\Delta H_{0,\,PCL}\cdot\omega_{PCL}}\times 100\% \quad (2)$$

Where ω_{PLA} and ω_{PLA} are the mass fraction of PLA and PCL in the blend respectively; $\Delta H_{m,\,PLA}$ and $\Delta H_{m,\,PCL}$ represent the melting enthalpy of PCL and PLA, respectively; $\Delta H_{c,\,PLA}$ is the cold crystallization enthalpy of PLA; $\Delta H_{0,\,PLA}$ (93J/g) and $\Delta H_{0,\,PCL}$ (139.3 J/g) are the complete crystallization enthalpy of PLA[40] and PCL,[41] respectively.

2.4 WAXD characterization

In order to investigate the crystallization orientation and structure of samples, the two-dimensional wide-angle x-ray diffraction (2D-WAXD) analysis was performed on the whole micropart and the shear layer of macropart along melt flow direction using the Bruker D8 Discover X-ray diffractometer (Bruker Company, Germany) in the azimuthal angular range of 0-360°. For macropart, the shear layer with 100 μm thickness is located 400 μm away from the surface. The used test conditions are below: wavelength of 0.15418 nm, voltage of 40 kV, current of 40 mA and scanning time of 180s.

2.5 FT-IR characterization

The Fourier transform infrared (FTIR) spectra of pure PLA, pure PCL and PLA/PCL blends were recorded at room temperature on a Nicolet 6700 Infrared spectrometer (Thermo Fisher Scientific Inc., USA) with a resolution of 4 cm^{-1}.

2.6 GPC measurement

The molecular weights of different samples were measured by using a HLC-8320 gel permeation chromatography (GPC) system (Tosoh Co., Japan) calibrated with narrow distribution polystyrene standard. The test was performed at 40 °C and chloroform was used as the eluent at a flow rate of 0.6 ml/min.

2.7 Tensile test

The tensile tests were conducted on PLA/PCL blend macroparts and dumbbell-shaped microparts at room temperature using an Instron universal testing machine 5567 (Instron Corporation, UK).

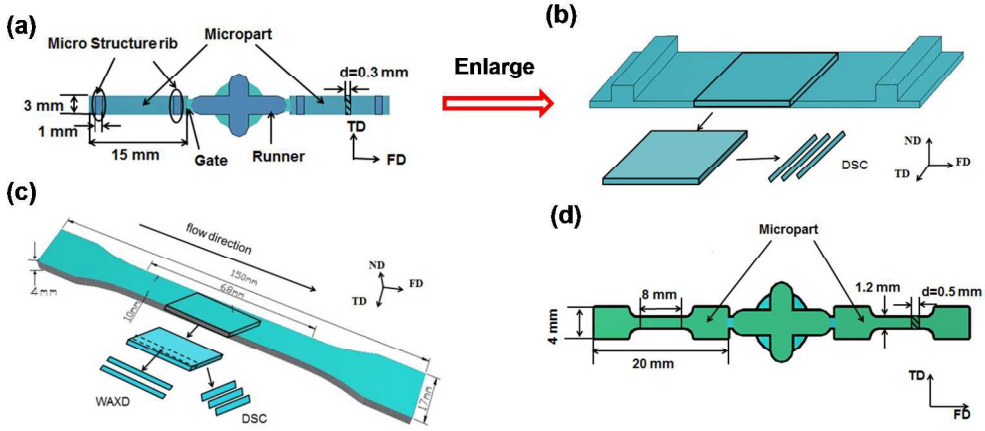

Fig. 1 The dimensions and sampling methods of micropart (a-b) and macropart (c); the dimensions of the dumbbell-shaped micropart (d). The whole micropart is used for WAXD analysis. FD: flow direction, TD: transverse direction and ND: normal direction

3. Results and Discussion

3.1 Morphology characterization

As we know, all dynamic molding process including injection molding would inevitably generate shear force and elongational stress fields. The shear force and elongation stress fields prove to have a very critical influence on the phase morphology of polymer blend. Generally, shear stress is beneficial to the dispersion of the dispersed phases to a certain extent. Under the effect of shear stress and elongational fields, the dispersed phase particles would be further deformed, elongated and finally broken into ellipsoids, fibers or smaller spheres.[42] It was reported that the shear rate of microinjection

molding processing could be as high as 10^6 s^{-1}. The resulted very strong shear force field will surely have a significant effect on the structure and morphology evolution of micropart. In order to investigate the effect of different injection molding methods on morphology and property, a series of characterizations including SEM and DSC were carried out.

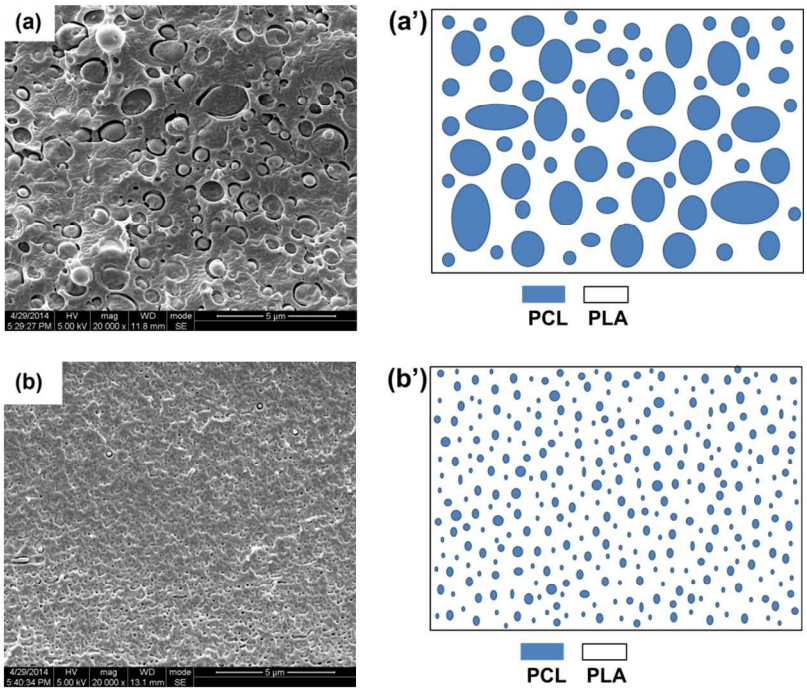

Fig. 2 SEM micrographs and schematic diagrams of the core layer at the fractured surface of PLA/PCL (80/20) blend macropart (a, a') and micropart (b, b') along cross-section direction

Fig. 2 shows the SEM photos of the core layer at the fractured surface (along perpendicular to the melt flow direction) of PLA/PCL blend samples prepared by conventional injection molding (a) and microinjection molding (b). The schematic diagrams show the distribution of PCL dispersed phases in PLA matrix. Fig. 3 compares the domain size distribution of PCL dispersed phase in macropart (a) and micropart (b) of PLA/PCL blends. It is interestingly found that there are substantial differences in the PCL dispersed phase morphology between conventional injection molded macropart and microinjection molded micropart. For macropart, almost all of the PCL dispersed phase exist in ellipsoid or sphere state in the cross-section direction. There are the obvious interfacial gaps between PCL particles and PLA matrix, indicating the poor interfacial compatibility. The domain size of PCL dispersed phase is in the range of 0.35 - 2.0 μm (averaged 0.76 μm). In addition, these PCL dispersed phases are unevenly distributed in PLA matrix. Comparatively, for micropart, the domain size of PCL dispersed phase is remarkably decreased and the size distribution becomes much narrower (most PCL dispersed phases are in the range of 50-250 nm and the averaged size is about 110 nm, where ~42% is in the nanometer range and ~53% is close to nanometer range), showing the great improvement in both the interfacial compatibility and the PCL dispersed phase dispersion. According to the subsequent SEM results of PCL dispersed phase along the melt flow direction, the PCL domain size is actually the diameter of the *in situ* formed PCL fibrils.

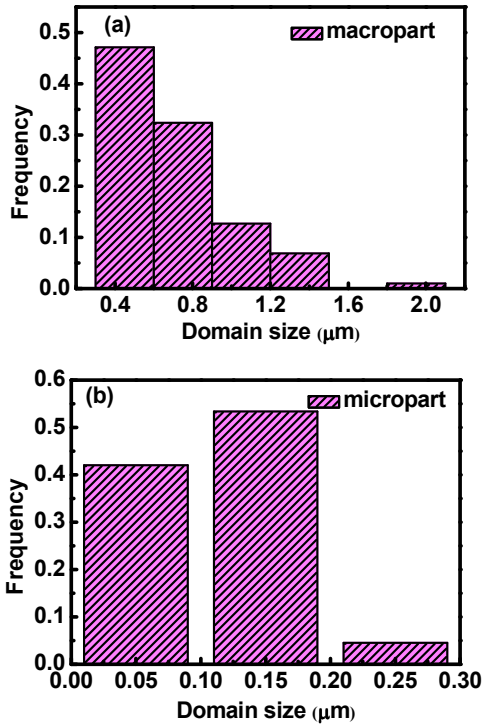

Fig. 3 The size distribution of PCL dispersed phase in PLA/PCL (80/20) blend macropart (a) and micropart (b)

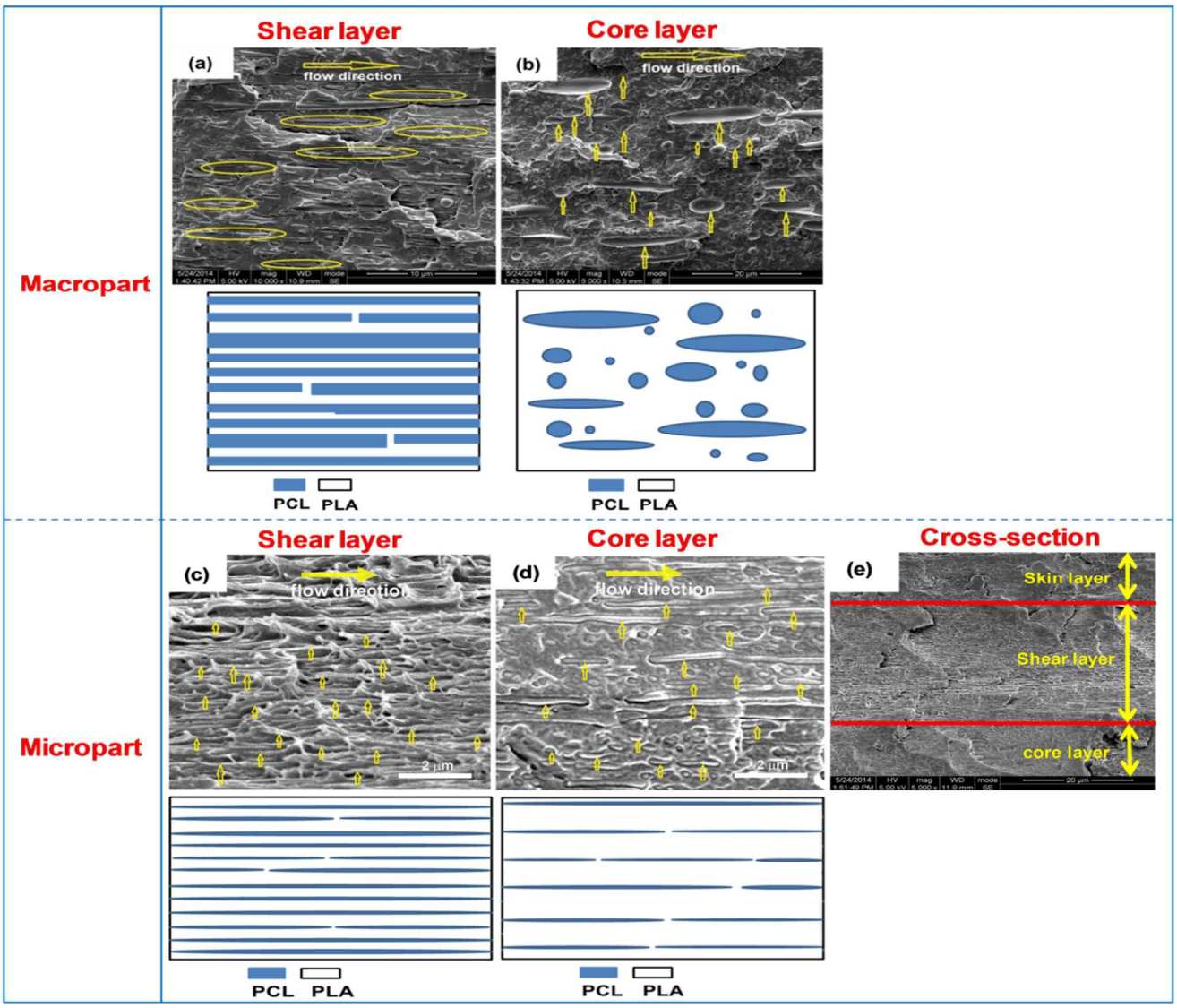

Fig. 4 SEM micrographs and schematic diagrams of PLA/PCL (80/20) blends: shear layer (a) and core layer (b) of macropart; shear layer (c), core layer (d) and cross-section of the fractured surface (e) of micropart along the flow direction

Fig. 4 shows the SEM micrographs of the fractured surface (along the melt flow direction) of PLA/PCL (80/20) blend macropart and micropart, where Fig. 4(a) and (b) show the morphology images of shear layer and core layer of macropart, respectively; Fig. 4(c), (d) and (e) show the morphology images of shear layer, core layer and the half fractured surface of micropart, respectively. As can be seen, in both macropart and micropart samples, at the fractured surface along the melt flow direction, there are skin-core structures appearing as skin layer, shear layer and core layer accordingly. In the shear and core layer regions of both samples, there are equally the orientation structures formed along the melt flow direction. For macropart, the spherical and elongated ellipse shape structures appear in the core layer, while the fibrillar structures oriented along the flow direction emerge in the shear layer. After measurement, the diameter of the fibrils in shear layer is in the range of 0.32-1.8 μm, which is consistent with the previous domain size result in cross-section direction (Fig. 2(a)). What is different from the macropart is that in micropart the PCL *in situ* nano-fibrillation phenomenon occurs in the almost whole micropart fractured surface (many PCL nanofibril structures appear in the shear layer and core layer except for skin layer) along the melt flow direction. After measurement, the diameter of the fibrils in shear layer is in the range of 48-220 nm, which is also in agreement with the previous domain size result (Fig. 2(b)). Comparatively, the *in situ* nano-fibrillation phenomenon in the shear layer is more remarkable and almost all the PCL dispersed phase particles are elongated into fibrils due to presence of the strongest shear force field there. This is because the shear layer of micropart is close to the mold cavity wall, which receives the greater shear force field. Accordingly, the low viscosity PCL (the viscosity of PCL at the processing temperature is much lower than that of PLA, indicating a high viscosity ratio) dispersed phase under the enhanced shear force field is more easily elongated into fibrils due to the interfacial tension.[43]

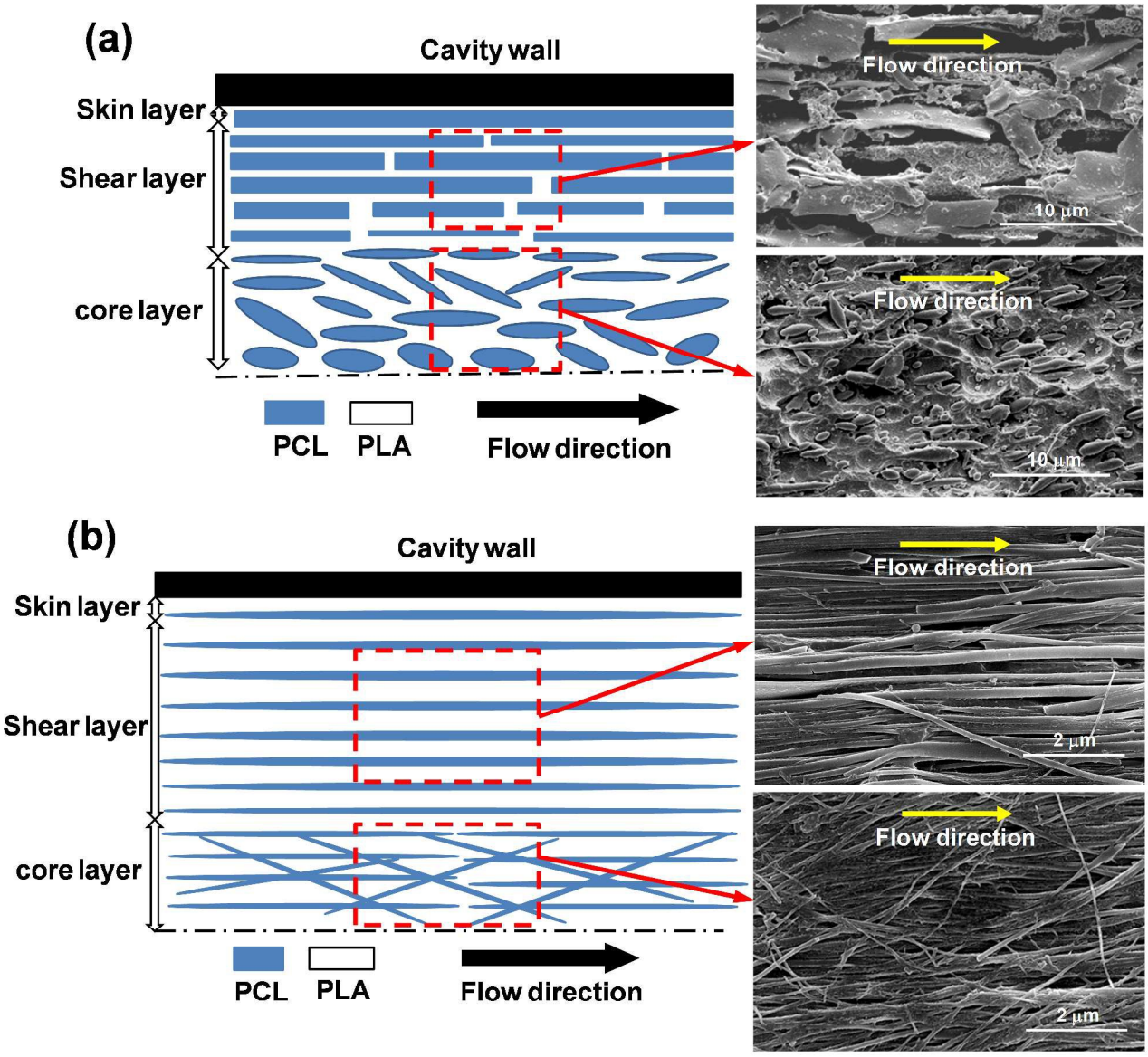

Fig. 5 The SEM micrographs and schematic diagrams of PLA/PCL (80/20) samples fractured surface etched with NaOH solution along the flow direction: macropart (a) and micropart (b)

In order to further confirm above results and more clearly observe the morphology evolution of the PCL phase, we applied the NaOH solution to remove part of the PLA phase. Fig. 5 shows the SEM micrographs and schematic diagrams of the etched fractured surface of PLA/PCL (80/20) macropart and micropart samples along the melt flow direction. Comparing Fig. 5(a) and (b), it is seen that in macropart sample the PCL dispersed phases exhibit the oriented fibrillar structures in shear layer and the less oriented spherical and ellipse shape structures in core layer. However, in micropart sample, it is very clear that there are the fibrils occurring in both shear layer and core layer. Relative to core layer, the formation and orientation of nanofibrils in shear layer is more significant. In shear layer, there are much more number of well-defined nanofibrils highly oriented along the melt flow direction. Comparatively, in the core layer, there are the relatively less number of well-defined nanofibrils oriented along the melt flow direction and the orientation degree is obviously reduced. The reason for the less orientation in core layer can be explained by the rheology existing in the polymer microinjection molding. As we know, for a polymer injection molding process, when the polymer melt is injected into a mold cavity, there is a shear rate distribution generated across the cross-section of the whole mold cavity, where the shear rate located at mold cavity wall tends to be maximum and the shear rate located at mold cavity center zone tends to be minimum. As a consequence, the polymer melt near the cavity wall would receive a much higher shear stress and the polymer melt near the cavity center zone would receive a much smaller shear stress. This means that the shear stress field near the cavity wall is much stronger than the

one near the cavity center zone. This would make the polymer melt near the cavity wall be extended along the melt flow direction much more easily than the one near the cavity center. On the other hand, the temperature gradient in the mold cavity also influences the orientation of polymer molecular chains. The melt temperature near the cavity center zone is much higher than the one near the cavity wall. Consequently, the stretched polymer melt near the cavity wall could be quickly solidified. However, the stretched polymer melt with viscoelasticity near the cavity center would recover to a certain degree through relaxation of molecular chains before solidification because of the still high melt temperature there, leading to the reduction in the orientation degree of polymer molecular chains. The schematic diagrams shown in Fig. 5 also demonstrate the morphology distribution of the macroparts and microparts. The results are in agreement with the findings previously obtained.

3.2 Morphology evolution mechanism

The remarkable difference in the morphology evolution between macropart and micropart can be explained by the great difference in the generated shear force field and the temperature gradient of polymer melt filled in mold cavity between microinjection molding and conventional injection molding. Generally, as far as an injection molding process (whether conventional injection or microinjection) is concerned, when the injection stage finishes, the dispersed phase would no longer receive shear stress but the interfacial tension would still be there. The deformed dispersed phase particles tend to return to their initial spherical states in order to reduce the interfacial energy. Because under the conventional injection molding conditions (for the macropart case), the shear force field is small, the degree of deformation and elongation of PCL dispersed phase is also small. As a result, under the effect of small shear force field, the dimension of the formed PCL dispersed phase tends to be big. On the other hand, the cooling temperature gradient of polymer melt in the macropart mold cavity is low (due to the big mold cavity size), resulting in the small cooling rate (the relationship between sample size and cooling rate will be illustrated in detail subsequently). This would make the elongated PCL particles easily recover to their original state and also have the enough time to undergo coalescence to form larger particles due to their viscoelasticity and the interfacial tension before cold solidification. However, under the microinjection molding conditions, the things are completely different. On one hand, relative to the conventional injection molding, the shear force field of microinjection molding becomes greatly enhanced. Under the very strong shear force field, the deformed and elongated PCL dispersed phase particles would be easily broken up into smaller particles and again extended quickly; On the other hand, under the microinjection molding conditions, the cooling temperature gradient of polymer melt is high due to the greatly reduced mold cavity size, leading to the high cooling rate. This would make the broken-up and then greatly extended PCL dispersed phase melt (in nanofibril form) quickly be frozen and solidified, resulting in much smaller domain size and more uniform domain size distribution. The morphology evolution mechanism for micropart and macropart above mentioned can be well illustrated using the following schematic diagram (Fig. 6).

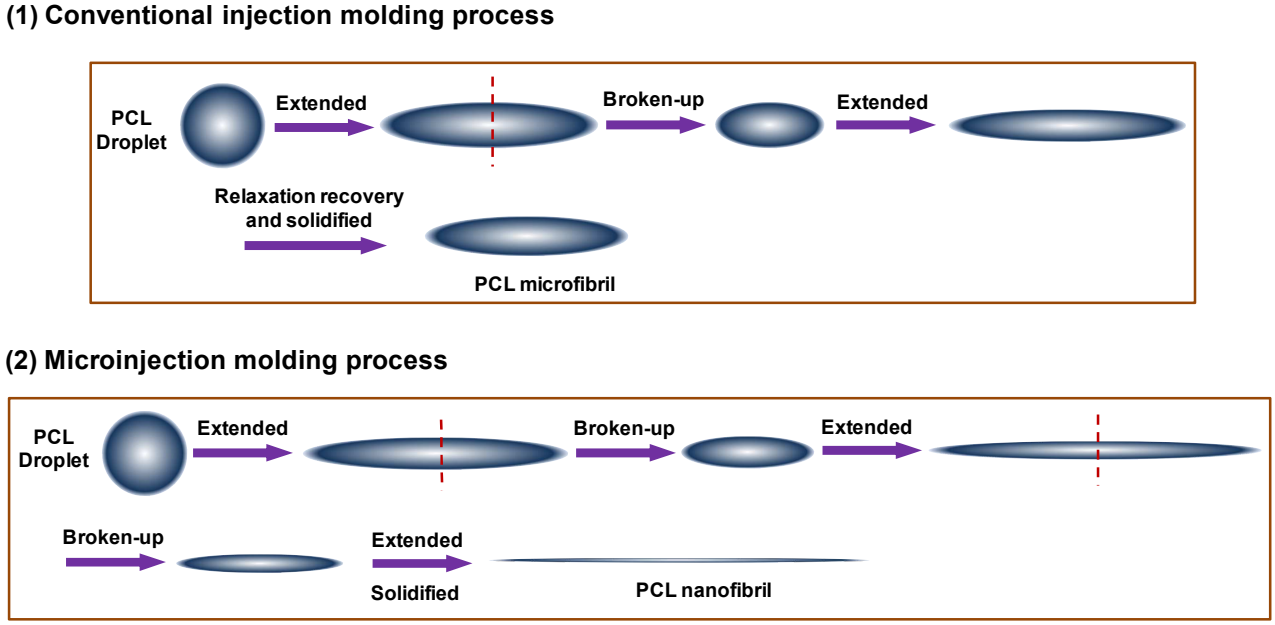

Fig. 6 The morphology evolution mechanism of PCL dispersed phase in PLA/PCL blends in microinjection molding and conventional injection molding process

To demonstrate how rapid the cooling rate is under microinjection molding and convention injection molding conditions, the temperature change in the two injection molding process during the cooling process was calculated according to the following equation:[21, 44]

$$T_{average} = T_{mold} + \frac{8}{\pi^2}(T_{melt} - T_{mold}) \exp\left(-\frac{\alpha\pi^2 t}{d^2}\right) \quad (3)$$

Where, $T_{average}$ is the real time average temperature of polymer melt, T_{mold} is the mold temperature, T_{melt} is the polymer melt temperature, d is the sample thickness and α is the thermal conductivity of the sample, which is about 0.205 mm^2/s for PLA materials (here the thermal conductivity of PLA was approximately regarded as the one of PLA/PCL blend). The obtained cooling curves are shown in Fig. 7. As can be seen, for micropart the real-time average temperature reaches the mold temperature within only 0.3s, while for macropart the similar cooling process takes more than 35s. This demonstrates that the cooling rate of micropart is almost about 120 times quicker than that of macroparts. Obviously, under microinjection molding conditions, at such a very rapid cooling rate, the sheared PCL particles with substantially reduced size could be immediately frozen and couldn't have time to return to their original state through relaxation.

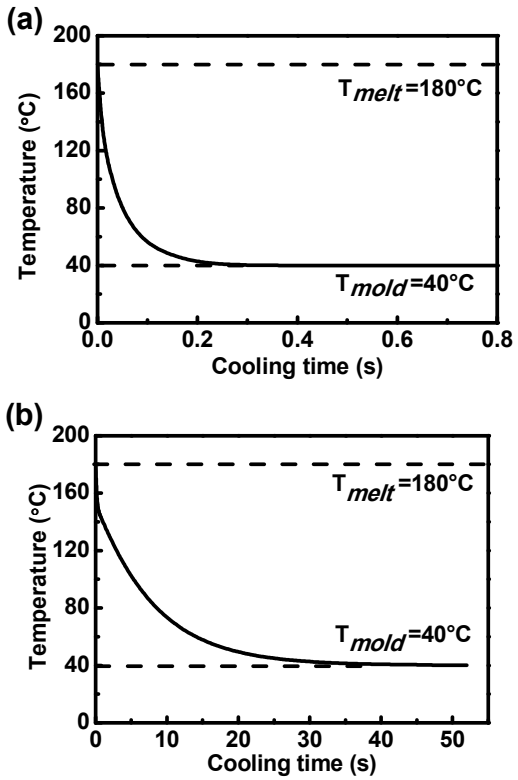

Fig. 7 Temperature profiles in the microparts (a) and macroparts (b) during the cooling process

Actually, the reasons for the PCL dispersed phase dimension of micropart being much smaller than that of macropart can also be illustrated by the research results of Guo-Hua Hu's group.[45] Hu et al found that in order to obtain a fine morphology for the blending of two immiscible polymers, the most favorable conditions should be: pellets melting/plasticization rate << dispersion rate (deformation + breakup) of the polymer melt to small particles << stabilization rate. Comparing conventional injection molding and microinjection molding, both have the similar pellets melting/plasticization rate. However, the latter has the much higher dispersion rate and stabilization rate than the former, because relative to conventional injection molding, microinjection molding has the much higher shear rate (much stronger dispersion effect on polymer melt droplets) and much higher cooling temperature gradient (this is helpful to the rapid solidification and stabilization of the polymer particles with reduced size due to the breakup of droplets).

3.3 Thermal analysis

Fig. 8 compares the DSC heating traces of PLA/PCL blends prepared under microinjection molding (micropart) and conventional injection molding (macropart) conditions, respectively. Previous studies[17, 21, 46-48] show that both macropart and micropart have skin-core structures containing skin layer, shear layer and core layer. These different layers may show different structures. So, it is interesting to investigate the melting and crystallization behavior of the different layer of PLA/PCL blend injection molded part. The DSC traces of the shear layer and core layer of macropart (not micropart) were accordingly recorded (the reason for not micropart results is that the micropart dimension is so small that the shear layer and core layer are very difficult to be sampled). The obtained results are also shown in Fig. 8. The corresponding DSC parameters are included in Table 1.

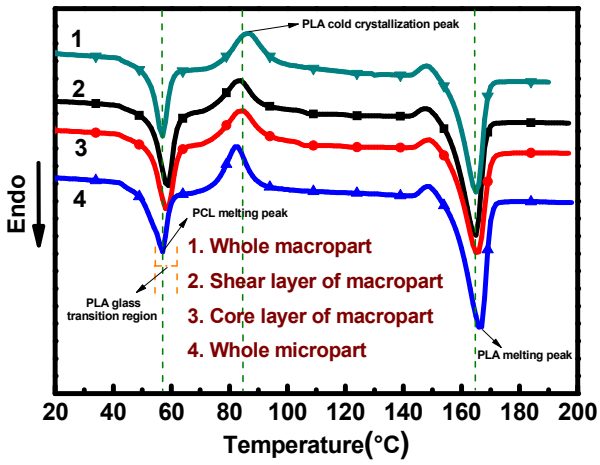

Fig. 8 The DSC heating curves of PLA/PCL (80/20) blend macropart and micropart samples

As can be seen, in the DSC curves of all samples, there are three peaks occurring. They are PCL melting endothermic peak (57°C), PLA cold crystallization exothermal peak (83°C) and PLA crystallization melting endothermic peak (166°C),

respectively. Since the glass transition of PLA occurs in the temperature range of 56-63°C, the PLA glass transition is overlapped with the PCL melting peak and the T_g of PLA cannot be identified. Comparing macropart with micropart, both have the similar PCL melting temperature, but the latter has the obviously higher crystallinity than the former (53.0% versus 44.4%). The reason for this may be that under microinjection molding conditions a relatively larger number of the formed PCL highly oriented fibrillar structures are arrayed into the crystal lattice, leading to increase in crystallinity. The cold crystallization is caused by a reorganization of macromolecular chains in the amorphous domains during the DSC heating process and the corresponding peak could reflect the crystallization capability of macromolecular chain segments to a certain degree. It is noted that, compared with macropart, micropart has the obviously lower cold crystallization peak temperature (82.5 °C versus 86.8 °C) and cold crystallization enthalpy. This indicates that the microinjection molding, on one hand, could hold back the cold crystallization of PLA in PLA/PCL blend system to a certain degree and, on the other hand, could promote the melt crystallization of PLA macromolecular chains. About results could be further verified by the significantly increased PLA crystallinity (from 16.1% to 27.0%, increased by ~70%) and the increased PLA melting temperature (from 165.1 °C to 166.5 °C) for micropart (compared with macropart). This is possibly because under microinjection molding conditions, the much stronger shear force field is more advantageous to the formation of PLA orientation structures which can enter the crystal lattice (the flow induced crystallization or shear induced crystallization[49]). For macropart, the different layer shows the different crystallization and melting behavior. It is noted that both shear layer and core layer show the obviously higher PCL melting temperature than the whole part and relative to core layer, shear layer also shows the slightly higher one. This is related to the different PCL orientation degree in different layer of macropart. Since there is the stronger shear force field in shear layer than in core layer, the PCL orientation degree in shear layer would be necessarily higher than in core layer (confirmed by the previous SEM results), leading to increase in the PCL melting temperature of shear layer. On the other hand, the whole macropart contains the amorphous skin layer and this would obviously decrease the averaged PCL melting temperature, even lower than that of core layer. The order of the cold crystallization temperature for different layer of macropart is found to be whole part>core layer>shear layer. This is related to formation of the oriented PCL fibrillar structures in shear layer and the existence of amorphous structures in skin layer of the whole part. From Fig. 8 and Table 1, it is also seen that like PCL, basically the PLAs in the shear layer and core layer of blend macropart also show the higher melting temperature than the whole part. In addition, particularly for PLA in the blend, the whole micropart even exhibits a lower cold crystallization temperature and an obviously higher melting temperature and crystallinity than the oriented shear layer of macropart. Above results verify that the shear force field generated under microinjection molding conditions is really much stronger than that generated under conventional injection molding conditions and is more beneficial to formation of oriented structures.

Table 1 The DSC parameters of PLA/PCL (80/20) blend macropart and micropart samples

Sample		T_{cc} (°C)	ΔH_{cc} (J/g)	T_m (°C)		ΔH_m (J/g)		$X_{c,PLA}$(%)	$X_{c,PCL}$(%)
		PLA	PLA	PLA	PCL	PLA	PCL		
Macropart	Whole part	86.8	17.47	165.1	56.9	29.47	12.36	16.13	44.36
	Shear layer	84.9	14.90	165.7	59.7	31.68	17.84	22.55	64.03
	Core layer	85.6	16.77	166.4	59.3	30.24	17.18	18.10	61.66
Whole micropart		82.5	16.19	166.5	56.9	36.29	14.76	27.02	52.97

3.4 WAXD analysis

In order to better understand the oriented crystalline structure, the 2D-WAXD measurement was conducted and the results are shown in Fig. 9. Regarding to the three samples we measured, the macropart shear layer is located at 400 μm away from the surface, while for ribbed micropart and dumbbell-shaped micropart, the whole part was used for test. As shown in Fig. 8, in the 2D-WAXD patterns of all the measured samples, there are two types of reflection patterns occurring, of which the outer reflection ring represents the PLA (015) crystal plane and the inner reflection ring or arcs represents the PCL (200) crystal plane. The reflection ring of PLA (015) crystal plane is so weak that it can hardly be identified and comparatively the reflection ring or arcs of PCL (200) crystal plane are much stronger. This shows that the PLA orientation in micropart and macropart of blend is much weaker than the corresponding PCL orientation. For macropart shear layer (Fig. 9(a)), there is a clear PCL (200) Debye ring occurring, indicating that the orientation of PCL even appearing in the shear layer of macropart is not significant. Comparatively, both the ribbed micropart and the dumbbell-shaped micropart show the strong PCL (200) crystal plane reflection arcs near the equator of the inner ring (the reflection results have been clearly illustrated in the schematic diagram), indicating that micropart prepared under microinjection molding conditions has the much higher orientation degree than macropart prepared under conventional injection molding conditions. The difference in the 2D-WAXD

result between micropart and macropart can be explained as follows. In general, the shear rate of microinjection molding conditions can be up to 2×10^6 s^{-1},[50] which is two orders of magnitude higher than that of conventional injection molding conditions. As a result, the shear force field in mold cavity under microinjection molding conditions is much stronger than that under conventional molding conditions. Therefore, the strong shear force field of microinjection molding more easily induces the PCL macromolecular chains to be oriented along the flow direction. Additionally, the temperature gradient under microinjection molding conditions is also much higher than that under conventional injection molding conditions, which can make the orientation structures fixed soon and have no enough time to restore their original state through relaxation. Above results are also in accordance with the SEM observations (Fig. 5), where the oriented PCL fibrils develop throughout the whole length of the micropart. From Fig. 9, it is also seen that in the reflection pattern of ribbed micropart, there are four strong shorter reflection arcs distributed at the both sides of the equator of the inner ring. However, in the reflection pattern of dumbbell-shaped micropart, there are two strong longer reflection arcs symmetrically distributed across the equator of the inner ring. It is known that the dumbbell-shaped micropart has a larger size than the ribbed micropart. This illustrates that the reduction in micropart size is beneficial to the orientation of PCL dispersed phase. This is because the micro mold cavity with decreased dimension could greatly enhance the shear force field. It can be predicted that the significant difference in the orientation structure will lead to the difference in mechanical properties.

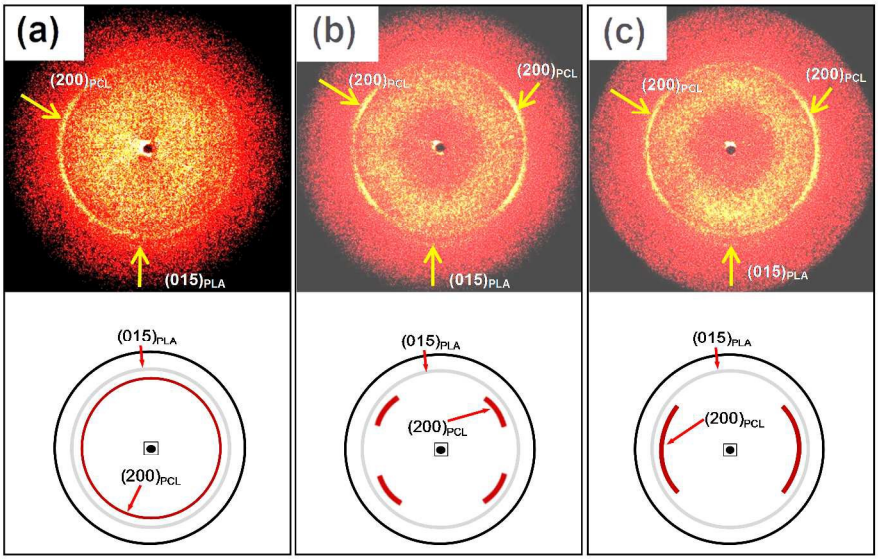

Fig. 9 The 2D-WAXD patterns and the corresponding schematic diagrams of PLA/PCL (80/20) blends: macropart shear layer (a), micropart with rib (b) and dumbbell shaped micropart (c), of which the dimension corresponds to Fig. 1(a), Fig. 1(c) and Fig. 1(d), respectively

3.5 Molecular characterization

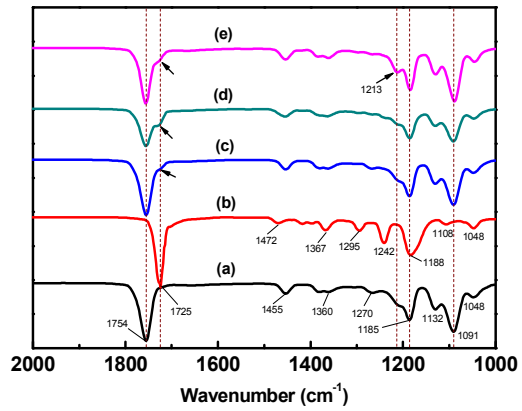

Fig. 10 FT-IR spectra of pure PLA (a), pure PCL (b), extruded PLA/PCL blend (c), conventional injection molded PLA/PCL blend (d) and microinjection molded PLA/PCL blend (e)

During processing, under the co-effects of heat and shear stress field, there are possible chemical changes occurring on polymers. So, it is interesting to investigate the structure change of PLA/PCL blend at molecular level.

Fig. 10 shows the FT-IR spectra of pure PLA, pure PCL, extruded PLA/PCL blend, conventional injection molded PLA/PCL blend (macropart) and microinjection molded PLA/PCL blend (micropart). As can be seen, for pure PLA, the strong peak at 1754 cm^{-1} and the bands in the range of 1050-1250 cm^{-1} can be attributed to the stretching vibration absorption of C=O and C–O–C in the ester group, respectively. In addition, the peaks at 1360 cm^{-1} and 1455 cm^{-1} can be ascribed to the stretching vibration absorption of –CH– and $–CH_3$ groups, respectively. For pure PCL, the peak at 1725 cm^{-1} is caused by the stretching vibration absorption of C=O group. The peaks at 1188 cm^{-1} and 1242 cm^{-1} are caused by the stretching vibration absorption of –C(=O)–O– group. The absorptions at 1472 cm^{-1} and 1295 cm^{-1} can be attributed to the vibration of $–(CH_2)_5–$ group. The absorptions at 1367 cm^{-1} and

1242 cm^{-1} can be ascribed to the vibration of –OH group. For the extruded and injection molded PLA/PCL blend (Fig. 10(c)-(e)), due to the low PCL content, most of absorptions of PCL functional groups are hidden by the absorptions of PLA functional groups. Only the featured absorption of C=O group of PCL at 1725 cm^{-1} appears as a shoulder in FT-IR spectra of PLA/PCL blend. There are no obvious differences in the main absorption peaks of PLA between the three PLA/PCL blend samples prepared by different processing method. This illustrates that there is possibly no transesterification occurring between PLA and PCL during processing, which is interesting and remains the further investigation later. In addition, it is noticed that in the FT-IR spectrum of micropart, there is a new weak peak appearing at 1213 cm^{-1}, which can be ascribed to the vibration absorption of C-O in carboxyl group. This indicates that during microinjection molding process part of PLA polymers possibly degrade to a certain degree under the shear stress field, which was confirmed by the further GPC characterization.

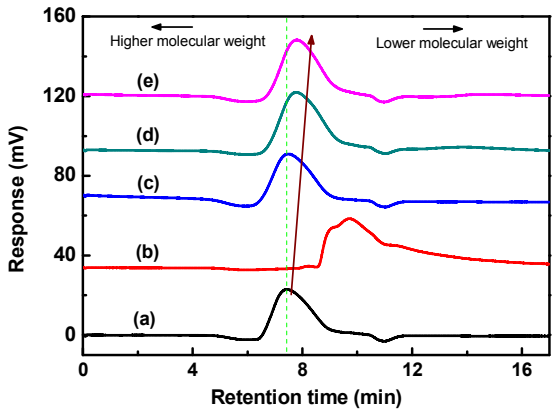

Fig. 11 The GPC curves of pure PLA (a), pure PCL (b), extruded PLA/PCL blend (c), conventional injection molded PLA/PCL blend (d) and microinjection molded PLA/PCL blend (e)

Fig. 11 shows the GPC results of pure PLA, pure PCL, extruded PLA/PCL blend, PLA/PCL macropart and PLA/PCL micropart. As can be seen, PLA shows a much higher molecular weight than PCL (the latter has an obviously longer elution time). This is consistent with the material information given by the experimental part. The GPC profile of PLA/PCL blend prepared by three different processing methods is more like that of pure PLA than the simple superposition of the elution curves of PLA and PCL. This indicates that there is possibly some interaction between PLA and PCL in PLA/PCL blend, which influences the elution of PCL. In addition, it is also noticed that from pure PLA, extruded PLA/PCL blend, macropart to micropart sample, the peak of the elution curve shifts toward longer time direction, indicating a decreasing tendency in molecular weight. This means that PLA degradation occurs during processing due to the co-effects of heat and shear stress field. Because there is the different intensity in the shear stress field of different processing method, the degradation degree of PLA is also different. The intensity of the shear stress field decreases in the order of microinjection molding>>conventional injection molding>extrusion. So, the decreasing degree of PLA molecular weight under microinjection molding condition would be at the maximum. This is in agreement with the FT-IR result. Compared with microinjection molding, the PLA degradation occurring under the other two processing conditions would become much less and hence it is difficult for the degradation products to be detected by the IR spectrometer. This is the reason why the weak peak at 1213 cm^{-1} does not appear in the FT-IR spectra of extruded blend (Fig. 10(c)) and macropart sample (Fig. 10(d)).

3.6 Mechanical performance

Fig. 12 compares the mechanical performance of the conventional injection molded macropart and the microinjection molded dumbbell-shaped micropart. It can be seen that the tensile strength, Young's modulus and elongation at break of micropart are all obviously higher than those of macropart (50.4 MPa versus 40.3 MPa, 2155MPa versus 1482 MPa and 46.0% versus 70.0%). Relative to macropart, the obvious enhancement in mechanical performance of micropart can be explained by the formed highly oriented structures (PCL nanofibrils), the increased crystallinity and the remarkable reduction in PCL domain size in micropart, which has been verified by the SEM observation, DSC measurement and 2D-WAXD results previously discussed. The result of elongation at break (a parameter which can be used to evaluate the toughness of material to a certain degree) is different from some of the previous results,[21, 51] where the macromolecular chains with a high orientation degree and the greatly enhanced crystallinity due to the high shear force field may result in poor toughness. The obvious improvement in the elongation at break is possibly related to the PCL nano-fibrillation occurring in micropart (Figs. 4-5).

Fig. 13 shows the tensile stress-strain curves of micropart and macropart. It can be seen that during the whole strain development process, the stress-strain curve of the dumbbell-shaped micropart is always located a lot above that of the macropart. It is very clear that the microinjection molded dumbbell-shaped micropart has the obviously higher tensile yield strength and elongation at break (toughness) than the conventional injection molded macropart. From Fig. 13, it can be also seen that the tensile stress-strain curves of both micropart and macropart show two platforms, which means a double yielding phenomenon.[52-53] Meanwhile, it is noted that for pure PLA micropart, there is no such double yielding phenomenon occurring. Above results indicate that the occurrence of the double yielding phenomenon for PLA/PCL blend micropart and macropart in tensile test should be related to presence of PCL in blend. From Fig. 13, it is also seen that the double yielding of the blend micropart is much remarkable than that of the blend macropart. According to the previous SEM results shown in Fig. 4, the difference in structure between blend micropart and macropart lies in such a fact that the number and the dimension of PCL fibrillar structures *in situ* formed in micropart is much more and smaller than that of macropart, respectively, which can hence explain the much

remarkable double yielding in micropart. As a result, it can be concluded that the double yielding phenomenon above mentioned is related to the PCL nano/micro-fibrillation occurring in blend micropart and macropart. In order to further investigate the double yielding phenomenon, the SEM observation was conducted on the fractured surface of PLA/PCL blend micropart after tensile test. The result is shown in Fig. 14. As can be seen, the tensile fractured surface of micropart is very rough and in the shear layer region, there are a lot of matrix resins drawn out. Particularly, it is noticed that a large sheet consisting of a great number of PCL fibrils is pulled out from the shear layer region upon tensile test. This can well explain the double yielding phenomenon for PLA/PCL blend micropart in tensile test.

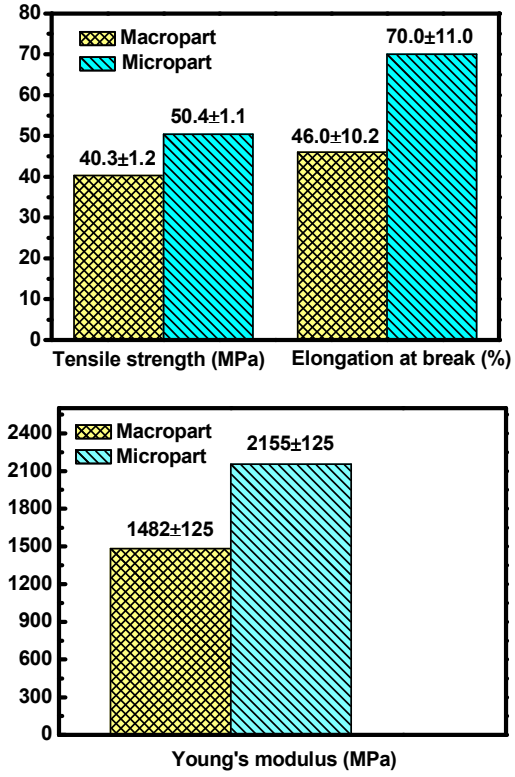

Fig. 12 The tensile strength, elongation at break and Young's modulus of conventional injection molded macropart and microinjection molded dumbbell-shaped micropart

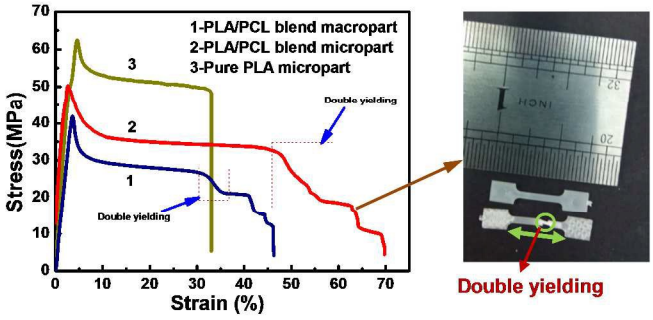

Fig. 13 The tensile stress-strain curves of conventional injection molded macropart and microinjection molded dumbbell-shaped micropart

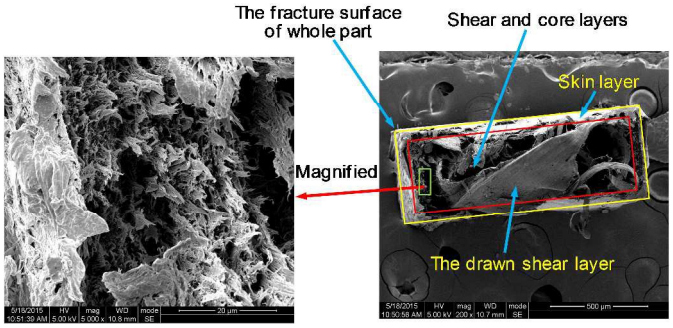

Fig. 14 SEM photos of the fracture surface of microinjection molded dumbbell-shaped micropart after tensile test

4. Conclusion

Microinjection molding was conducted on PLA/PCL blend, an interesting system combining the advantages of PLA and PCL, e.g. the biodegradability, biocompatibility, good formability, good strength of PLA, good toughness of PCL, etc. For comparison, conventional injection molding was also carried out. Compared with conventional injection molding, under microinjection molding conditions, the domain size of PCL dispersed phase in cross-section direction is substantially decreased (from 0.35-2.0 μm to 50-250 nm), the domain size distribution is narrowed and the interfacial compatibility becomes better. Both PLA/PCL blend micropart and macropart show the skin-core structure appearing as skin layer, shear layer and core layer. Very interestingly, in the shear layer and core layer of micropart, there are PCL nanofibrils (48-220 nm) *in situ* formed and highly oriented along melt flow direction, i.e. existing nano-fibrillation phenomenon. However, for macropart, there are only PCL microfibrils (0.32-1.8 μm) *in situ* formed, i.e. showing micro-fibrillation. The substantial difference in PCL dispersed phase dimension between micropart and macropart can be ascribed to such a fact that microinjection molding possesses the much stronger shear force field and much higher cooling rate (temperature gradient) than conventional injection molding. In addition, for the different location in the same sample, the degrees of PCL nano/micro-fibrillation and orientation in blend are different. The SEM observation and WAXD results show that for both micropart and macropart, the shear layer have the much higher degrees of PCL nano/micro-fibrillation and orientation than the core layer. The reason for this can be explained by the much stronger shear force field in shear layer than in core layer. In addition, it is also found that relative to macropart, micropart has the increased PCL crystallinity and the remarkably enhanced PLA crystallization capability (much lower cold crystallization temperature, much higher crystallinity and higher melting temperature). Molecular characterizations show that under the co-effects of heat and shear stress field, PLA would degrade and the microinjection molded blend exhibits the highest degradation degree. The PLA/PCL blend micropart also shows much higher tensile yield strength, Young's modulus and elongation at break than macropart, which is explained by PCL

nano-fibrillation and orientation. There is the double yielding phenomenon occurring in both micropart and macropart and comparatively, micropart result is much more remarkable.

Acknowledgments

We would like to express our great thanks to the National Natural Science Foundation of China (51421061; 5143006), the International Science and Technology Cooperation Program of China (2013DFG52300) and the Program of Introducing Talents of Discipline to Universities (B13040) for financial support.

Notes and references

1. U. M. Attia, S. Marson and J. R. Alcock, *Microfluidics and Nanofluidics*, 2009, **7**, 1-28.
2. J. Zhang, C. Guo, X. Wu, F. Liu and X. Qian, *Journal of Macromolecular Science, Part B: Physics*, 2011, **50**, 2227-2241.
3. M. Heckele and W. K. Schomburg, *Journal of Micromechanics and Microengineering*, 2004, **14**, R1-R14.
4. C. Yang, X. H. Yin and G. M. Cheng, *Journal of Micromechanics and Microengineering*, 2013, **23**, 093001.
5. A. Y. Yi, W. Lu, D. F. Farson and L. J. Lee, *Advances in Polymer Technology*, 2008, **27**, 188-198.
6. W. Michaeli, D. Opfermann and T. Kamps, *The International Journal of Advanced Manufacturing Technology*, 2007, **33**, 206-211.
7. P. Deng, B. Whiteside, F. Wang, K. Norris and J. Zhang, *Polymer Testing*, 2014, **34**, 192-201.
8. W. B. Young, *Applied Mathematical Modelling*, 2007, **31**, 1798-1806.
9. C. A. Griffiths, S. S. Dimov, E. B. Brousseau and R. T. Hoyle, *Journal of Materials Processing Technology*, 2007, **189**, 418-427.
10. L. Wang, Q. Li, W. Zhu and C. Shen, *Microsystem Technologies*, 2012, **18**, 2085-2091.
11. M. Mahmoodi, S. S. Park and G. Rizvi, *Polymer Engineering & Science*, 2012, **52**, 180-190.
12. K. F. Zhang and Z. Lu, *Microsystem Technologies*, 2008, **14**, 209-214.
13. C. K. Huang, *European Polymer Journal*, 2006, **42**, 2174-2184.
14. M. R. Mani, R. Surace, P. Ferreira, J. Segal, I. Fassi and S. Ratchev, *Journal of Micro and Nano-Manufacturing*, 2013, **1**, 031003.
15. Z. Jiang, Y. Chen and Z. Liu, *Journal of Polymer Research*, 2014, **21**, 451-465.
16. P. Deng, K. Liu, L. Zhang, H. Liu, T. Wang and J. Zhang, *Journal of Macromolecular Science, Part B: Physics*, 2014, **53**, 24-39.
17. F. Liu, C. Guo, X. Wu, X. Qian, H. Liu and J. Zhang, *Polymers for Advanced Technologies*, 2012, **23**, 686-694.
18. C. Guo, F. H. Liu, X. Wu, H. Liu and J. Zhang, *Journal of Applied Polymer Science*, 2012, **126**, 452-462.
19. A. C. Liou and R. H. Chen, *International Journal of Advanced Manufacturing Technology,* 2006, **28**, 1097-1103.
20. H. X. Huang, Z. Wu, W. S. Guan and B. Wang, *Acta Polymerica Sinica*, 2013, **12**, 1514-1519.
21. Y. M. Pan, S. Y. Shi, W. Z. Xu, G. Q. Zheng, K. Li Dai, C. T. Liu, J. B. Chen and C. Y. Shen, *Journal of Materials Science*, 2014, **49**, 1041-1048.
22. X. Lin, F. Caton-Rose, D. Ren, K. Wang and P. Coates, *Journal of Polymer Research*, 2013, **20**, 122(1-12).
23. M. R. Kamal, J. Chu, S. Derdouri and A. Hrymak, *Plastics, Rubber and Composites*, 2010, **39**, 332-341.
24. J. Giboz, T. Copponnex and P. Mélé, *Journal of Micromechanics and Microengineering*, 2009, **19**, 025023(1-12).
25. K. Takahiko, R. Nelly, M. Go, N. Koji, K. Toshiji, N. Mitsuru, O. Hirotaka, K. Jumpei, U. Arimitsu, H. Nobutaka, N. Katsuhiko and M. Masatoshi, *Macromolecules*, 2007, **40**, 9463-9469.
26. K. Kim, M. Yu, X. Zong, J. Chiu, D. Fang, Y. S. Seo, B. S. Hsiao, B. Chu and M. Hadjiargyrou, *Biomaterials*, 2003, **24**, 4977-4985.
27. E. Saito, E. E. Liao, W. W. Hu, P. H. Krebsbach and S. J. Hollister, *Journal of Tissue Engineering and Regenerative Medicine*, 2013, **7(2)**, 99-111.
28. A. Salerno, M. Fernández-Gutiérrez, J. S. R. del Barrio and C. D. Pascual, *RSC Advances*, 2014, **4**, 61491-61502.
29. H. Xu, G. J. Zhong, Q. Fu, J. Lei, W. Jiang, B. S. Hsiao and Z. M. Li, *ACS Applied Materials & Interfaces*, 2012, **4(12)**, 6774-6784.
30. W. K. Chee, N. A. Ibrahim, N. Zainuddin, M. F. Abd Rahman and B. W. Chieng, *Advances in Materials Science and Engineering*, 2013, 97673(1-8).
31. J. B. Zeng, K. A. Li and A. K. Du, *RSC Advances*, 2015, **5**, 32546-32565.
32. M. Singhvi and D. Gokhale, *RSC Advances*, 2013, **3**, 13558-13568.
33. N. Noroozi, L. L. Schafer and S. G. Hatzikiriakos, *Polymer Engineering & Science*, 2012, **52**, 2348-2359.
34. C. C. Chen, J. Y. Chueh, H. Tseng, H. M. Huang and S. Y. Lee, *Biomaterials*, 2003, **24(7)**, 1167-1173.
35. J. T. Yeh, C. J. Wu, C. H. Tsou, W. L. Chai, J. D. Chow, C. Y. Huang, K. N. Chen and C. S. Wu, *Polymer-Plastics Technology and Engineering*, 2009, **48**, 571-578.
36. T. Semba, K. Kitagawa, U. S. Ishiaku and H. Hamada, *Journal of Applied Polymer Science*, 2006, **101**, 1816-1825.
37. L. Chen, J. Yang, K. Wang, F. Chen and Q. Fu, *Polymer International*, 2010, **59**, 1154-1161.
38. H. Bai, H. Xiu, J. Gao, H. Deng, Q. Zhang, M. Yang and Q. Fu, *ACS Applied Materterials & Interfaces*, 2012, **4**, 897-905.
39. H. Bai, C. Huang, H. Xiu, Y. Gao, Q. Zhang and Q. Fu, *Polymer*, 2013, **54**, 5257-5266.
40. M. Shibata, Y. Inoue and M. Miyoshi, *Polymer*, 2006, **47**, 3557-3564.
41. G. M. V. Crescenzi, G. Calzolari , C. Borri, *European Polymer Journal*, 1972, **8**, 449-463.
42. E. S. Chris and W. M. Christopher, *Polymer*, 1995, **36**, 461-470.
43. S. Takeshi, K. Kazuo, E. Satoshi, M. Kazunori and H. Hamada, *Journal of Applied Polymer Science*, 2004, **91**, 833-840.
44. A. Frick, C. Stern, G. Michler, S. Henning and M. Ruff, *Macromolecular Symposia*, 2010, **294**, 91-101.
45. H. X. Li and G. H. Hu, *Journal of Polymer Science, Part B: Polymer Physics*, 2001, **39**, 601-610.
46. C. Tan, S. Bai and Q. Wang, *Journal of Applied Polymer Science*, 2014, **131**, 40538(1-12).
47. B. A. G. Schrauwen, L. C. A. V. Breemen, A. B. Spoelstra, L. E. Govaert, G. W. M. Peters and H. E. H. Meijer, *Macromolecules*, 2004, **37**, 8618-8633.
48. Z. Zhao, Q. Yang, S. Xi, M. Kong, Y. Huang and X. Liao, *RSC Advances*, 2015, **5**, 61127-61136.
49. G. Lamberti, *Chemical Society Reviews*, 2014, **43**, 2240-2252.
50. N. Zhang, S. Y. Choi and M. D. Gilchrist, *Macromolecular Materials and Engineering*, 2014, **299**, 1362-1383.
51. Z. Liu, Y. Chen, W. Ding and C. Zhang, *Composites Part A: Applied Science and Manufacturing*, 2015, **72**, 85-95.
52. J. L. Pan and Z. M. Li, *Journal of Applied Polymer Science*, 2008, **108**, 287-294.
53. Z. M. Li, W. Yang, B. H. Xie, R. Huang, M. B. Yang and J. M. Feng, *Journal of Macromolecular Science, Part B: Physics*, 2004, **43**, 519-542.

During microinjection molding, there are highly oriented PCL nanofibrils *in situ* formed, while during conventional injection molding, there are oriented microfibrils *in situ* formed.